Fuller, J. D., Jalalvand, M., & Wisnom, M. R. (2015). Analytical modelling of pseudo-ductility in angle-ply CFRP laminates with central unidirectional plies. Paper presented at 20th International Conference on Composite Materials (ICCM20), Copenhagen, Denmark.

20th International Conference on Composite Materials
Copenhagen, 19–24th July 2015

ANALYTICAL MODELLING OF PSEUDO-DUCTILITY IN ANGLE-PLY CFRP LAMINATES WITH CENTRAL UNIDIRECTIONAL PLIES

Jonathan Fuller*, Meisam Jalalvand, Michael R Wisnom

Advanced Composites Centre for Innovation and Science, University of Bristol, BS8 1TR, UK
*Email: J.D.Fuller@bristol.ac.uk, website: www.hiperduct.ac.uk

Keywords: Pseudo-ductility, Angle-ply, Thin ply

ABSTRACT

A new analytical modelling method is developed and subsequently used to predict the pseudo-ductile, metal-like stress-strain responses of thin ply CFRP $[\pm\theta/\underline{0}]_s$ laminates. Three combinations of thin ply materials containing standard (235 GPa) and high (540 GPa, 720 GPa, 780 GPa) modulus fibres have been utilised. The modelling method is used to determine the range of $\pm\theta$ values for each material combination that will exhibit pseudo-ductility. It is shown that a high modulus 0° ply and standard modulus $\pm\theta$ layers can produce considerable pseudo-ductility, via fragmentation of the 0° ply and local delaminations at the 0/-θ interfaces. With the use of the various thin ply materials and a range of $\pm\theta$ angles between 20°–30°, the stress-strain response of these laminates can be finely controlled to achieve a desired 'yield' stress plateau, pseudo-ductile strain or laminate strength.

1 INTRODUCTION

Carbon fibre reinforced polymers (CFRP) are well known to be limited by their inherent lack of ductility, often exhibiting a linear-elastic, brittle failure. This brittle behaviour means that large safety factors have to be employed in structural design of CFRP, greatly limiting the efficiency of the solution. Recent work, as part of the High Performance Ductile Composite Technologies (HiPerDuCT) programme grant, has shown that it is possible to achieve highly non-linear tensile stress-strain behaviour via the use of thin ply CFRP prepreg materials [1–5].

Thin ply angle-ply laminates (ply thickness, t_p = 0.03 mm) have been shown in [1, 4] to effectively suppress the damage mechanisms — matrix cracking and free-edge delaminations — that commonly cause failure of angle-ply laminates with a standard ply thickness of 0.125 mm [6–9]. This damage suppression allows the matrix to deform plastically, leading to considerable fibre rotations, which in turn contribute to the development of pseudo-ductility. In this paper, 'pseudo-ductility' is due to the gradual failure of central 0° plies and geometric effect of fibre reorientation, as well as yielding of the matrix. The pseudo-ductile strain is defined as the failure strain minus the strain at the same stress level on a straight line of the initial modulus. The parameter 'yield' stress, σ_Y, is defined by the level of stress at the point of fragmentation.For example, experimental results for a $[\pm 30_5]_s$ layup yield a mean pseudo-ductile strain, ε_d, of 2.88%, a failure strain, ε_x^*, of 5.40% with a strength, σ_x^*, of 727 MPa.

Work by Czél, Jalalvand and Wisnom [2, 10] has shown that is also possible to achieve pseudo-ductile stress-strain behaviour using unidirectional hybrid laminates of standard thickness glass fibre reinforced polymer (GFRP) with thin ply CFRP, in a $[G_n/C_m/G_n]$ configuration. The thin ply CFRP suppresses the delaminations that normally occur in hybrid laminates [11–13], allowing a gradual failure of the CFRP plies via fragmentation. The work in [2, 5, 10] also highlighted that the damage development is sensitive to both the absolute and the relative thickness of the CFRP. The values of m and n can be carefully 'tuned' to give the optimal stress-strain response. The standard thickness GFRP, however, limits this, effectively constraining performance.

Replacing the standard thickness GFRP plies with thin CFRP plies oriented at $\pm\theta$, has been shown in [3] to allow more precise control of the failure process. Laminates of $[\pm 26_5/0]_s$ displayed a metal-like

stress-strain curve, giving a mean $\varepsilon_d = 2.22\%$, $\varepsilon_x^* = 4.20\%$ and $\sigma_x^* = 801$ MPa. Microscopy and ultrasound C-scanning were able to demonstrate that periodic fragmentations of the zero plies occur, which led to local delaminations at the $0/-26$ interfaces. Similarly to the results of the angle-ply laminates discussed above, the $\pm\theta$ plies were shown to be free of damage.

The optimal solution for this concept is to reduce the laminate thickness by as much as possible. This can be done by maximising the stiffness mismatch between the 0° and $\pm\theta$ plies. Using North Thin Ply Technology (NTPT) CFRP, with high modulus fibres, such as Toray M55J (fibre modulus, E_f = 540 GPa [14]), Nippon XN-80 (E_f = 780 GPa [15]) and Nippon YSH-70A (E_f = 720 GPa [16]), presents the opportunity to progress the work discussed above with layups of $[\pm\theta/\underline{0}]_s$. Analytical predictions of these layups are presented here, using a non-linear method based on those described in [5] and [4]. The various layup combinations are compared, illustrating the degree of control this technique has over parameters such as initial laminate modulus, E_{xi}, σ_x^*, σ_Y and ε_d.

2 ANALYTICAL MODELLING PROCEDURE

The methods that form the basis of the analysis conducted in this work are discussed in detail in [4,5,17], so only the key points of the process are presented here. The method, coded using MATLAB®, is non-linear and iterative, taking account of the matrix plasticity and fibre rotations that occur in the $\pm\theta$ plies, as in [4].

The method detailed in [4] has been augmented by incorporating the possible failure modes that may take place in a hybrid laminate, as set out by Jalalvand et al. [5]. There are three possible modes of failure that can occur: fragmentation of the 0° plies; delamination of the $0/-\theta$ interface, and failure of the $\pm\theta$ plies. The stress-strain response is linear-elastic in the fibre direction, so once the fibre direction ply stress, σ_{11}, increases to the point that the inequality $\sigma_{11}/E_{11} \geq \varepsilon_{11}^*$ is satisfied, the first failure in the 0° plies is deemed to have occurred. E_{11} and ε_{11}^* are the modulus and strain to failure of the material in the fibre direction. The subsequent behaviour of the laminate depends on the relative strengths and thickness of the 0° and $\pm\theta$ plies. If the strength of the angle-ply is sufficient to withstand the stress redistribution created by the UD failure, then further strain can be taken by the laminate. If, however, the angle-ply is not sufficiently strong, then complete failure of the specimen will occur without the development of any non-linearity.

2.1 FRAGMENTATION

Shown in Figure 1, a unit cell approach, which assumes the damage to be symmetric about the mid-plane, is taken to calculate the stress in the angle-ply layers at the point of 0° fracture and then compare that with a known strength for that $\pm\theta$ layup. The stress in the angle-plies away from the 0° fracture is denoted as σ_x^{AP}. The stress at the crack, σ_{crack}, is calculated using the effective reduced cross-section of the laminate after the fracture of the UD plies. A stress concentration factor of $K_t = 1.08$, as used in [5], is included to account for the local stress increase at the crack tip.

$$\sigma_{crack} = K_t \sigma_x \left(\frac{t}{t_{\mathrm{AP}}} \right) \tag{1}$$

Where σ_x is the laminate applied stress, t_{AP} is the thickness of the angle-ply layers and t is the laminate thickness ($t = (t_{\mathrm{AP}} + t_{\mathrm{UD}})$), noting that, due to symmetry, these pertain to the half thickness. The value of σ_{crack} is then compared to the known strength for that $\pm\theta$ layup, determined as per the model described in [1].

If failure of the laminate does not occur at this point, then further fragmentations will develop in regions of uniform stress. This, coupled with the assumption of a constant fibre direction strength means that the global stress, σ_x, remains constant as fragmentations develop. The spacing of these fragmentations is defined as the critical length, l_c. Assuming that the matrix is an elastic-plastic material giving a

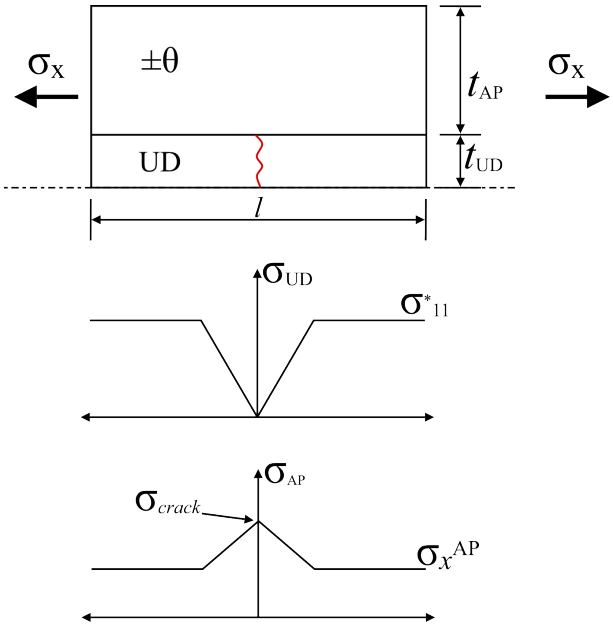

Figure 1: The unit cell, with a single fracture in the 0° plies, is shown. The graphs below indicate the idealised redistribution of stresses in the 0° and $\pm\theta$ layers.

constant shear stress at the interface (τ_Y = 55 MPa [1]), l_c can be found by:

$$l_c = \frac{2\sigma_{11}^{*} t_{\mathrm{UD}}}{\tau_Y} \tag{2}$$

It can be seen from Equation 2 that l_c is dependent on the thickness of the UD plies and the strengths of the material in the fibre direction and in interfacial shear. Saturation of fragmentations occurs when the stress in the 0° plies is no longer uniform at any point along the length of the laminate and the material is broken into pieces of length between $l_c/2$ and l_c [11].

2.2 DELAMINATION

Due to the fractures in the 0° plies, Mode II delamination may occur at the 0/-θ interfaces [18]. The stress at which this delamination occurs is governed by Equation 3, which is adapted from [5].

$$\sigma_{del} = \frac{1}{t_{\mathrm{AP}} + t_{\mathrm{UD}}} \sqrt{\frac{2G_{IIc} E_x^{\mathrm{AP}} t_{\mathrm{AP}} (E_x^{\mathrm{AP}} t_{\mathrm{AP}} + E_{11} t_{\mathrm{UD}})}{E_{11} t_{\mathrm{UD}}}} \tag{3}$$

Where G_{IIc} is the critical strain energy release rate for Mode II delamination. An initial value of G_{IIc} = 1.0 N/mm has been established for the Skyflex USN020A used in [2] and [5]. The NTPT material has been found to have a lower toughness, with a G_{IIc} = 0.5 N/mm [19].

The value of σ_{del} does not remain constant over the course of the loading, as the non-linearity of the angle-plies leads to a reduction in E_x^{AP}, the secant modulus of the angle-plies.

If σ_{del} is less than or equal to the value of σ_{frag} at the point of initial fragmentation (ε_{frag}), then a large single delamination will occur at the $0/-\theta$ interface. This delamination is undesirable, as it causes a large load drop at the point of initial fragmentation. The laminate continues to take load, but at a lower level and its integrity is heavily diminished [2]. Conversely, if $\sigma_{frag} = \sigma_{del}$ at $\varepsilon_x > \varepsilon_{frag}$, rather than a single delamination, many dispersed delaminations will occur local to the multiple fragmentations. It is assumed in the model that these delaminations will propagate until the 0° plies cease to carry any load.

2.3 FAILURE OF $\pm\theta$ PLIES

The failure of angle-ply layers depends on the the absolute and relative thickness of the 0° plies. If the thickness or proportion of 0° plies in the laminate is too large then the stress offloaded to the angle-ply layers at failure of the 0° will be in excess of the angle-ply strength, σ^*_{AP}. An estimate of the maximum value of the thickness ratio, B_{max}, can be made using Equation 4 below, which is adapted from [5] and comes from the need for σ_{frag} to be less than σ^*_{AP}.

$$B_{max} = \frac{\sigma^*_{\mathrm{AP}}}{\sigma^*_{11}} - \frac{E_x^{\mathrm{AP}}}{E_{11}} \tag{4}$$

This relationship shows that the maximum relative thickness of 0° plies for a given value of $\pm\theta$ is governed by the ratio of angle-ply:UD strength and stiffness. The initial value of E_x^{AP} is used to give a conservative measure of B_{max}.

It is assumed in the model that, after saturation, the angle-plies are carrying the majority of the load. Indeed, following complete delamination of the UD plies, the angle-plies take all the applied load. Laminate failure is deemed to have occurred if the following is true:

$$\sigma^*_{\mathrm{AP}} \leq \sigma_{\mathrm{AP}} = \sigma_x \frac{t}{t_{\mathrm{AP}}} \tag{5}$$

If the above is satisfied, the model halts without additional increments and stores all relevant stress-strain data.

3 ANALYTICAL PREDICTIONS

With the modelling procedure in place, predictions have been performed for $[\pm\theta/\underline{0}]_s$ laminates with various material combinations and $\pm\theta$ angles. Introduced above, NTPT materials containing high modulus carbon fibres (Toray M55J, Nippon XN-80, YSH-70A) have been used for the 0° plies. All the NTPT materials are modelled assuming a fibre volume fraction, v_f, of 50%. The material that forms the angle-ply layers has remained unchanged throughout, using Skyflex USN020A prepreg. The material properties of each are listed in Table 1. The G_{IIc} of 0.5 N/mm for the NTPT material is lower than the Skyflex, so this value has been used in Equation 3.

Table 1: The elastic constants for all materials used in the $[\pm\theta/\underline{0}]_s$ laminates.

	E_{11} [GPa]	E_{22} [GPa]	G_{12} [GPa]	ν_{12}	σ^*_{11} [MPa]	ε^*_{11} [%]	t_p [mm]
Skyflex	101.7	6.0	2.4	0.3	1940	1.9	0.03
M55J	280	6.2	5.0	0.25	2200	0.8	0.032
XN-80	392	5.0	4.0	0.3	1960	0.5	0.046
YSH-70A	362	6.0	4.0	0.3	1810	0.5	0.03

An initial range of $\pm\theta$ fibre angles between 20°–30° has been selected for each material pairing. This range was demonstrated in [1] to provide the a good balance between initial laminate modulus, strength and pseudo-ductile strain. Not all angles in the range are applicable to every material pairing, as Table 2 shows. For the selected material combinations, in order for a laminate of $[\pm\theta/\underline{0}]_s$ to be viable, the values of B_{max} are as follows:

- M55J—Skyflex — $B_{max} \geq 0.26$
- XN-80—Skyflex — $B_{max} \geq 0.38$

- YSH-70A—Skyflex — $B_{max} \geq 0.25$

Table 2 shows that it is not possible to achieve pseudo-ductility from the entire range of $\pm\theta$ values. The M55J and XN-80 fibre combinations are limited to a maximum fibre angle of $\pm 24^\circ$; whilst the YSH-70A allows a much wider scope of layups, up to $\pm 29^\circ$. The values of B_{max} for the YSH-70A—Skyflex layups also indicate that, for fibre angles less than $\pm 24^\circ$, half the amount of angle-plies could be used and pseudo-ductility would still be achieved. The $\pm 24^\circ$ layup, however, is not optimal, as the increased value of B_{max} suggests that the 'yield' stress will be much lower than the laminate strength.

Table 2: The maximum thickness ratios, B_{max}, for NTPT—Skyflex combinations over a range of 20°–30° $\pm\theta$ fibre angles.

$\pm\theta$	20	21	22	22.5	23	24	25	26	27	28	29	30
M55J/Skyflex	0.37	0.38	0.38	0.39	0.38	0.34	0.26	0.24	0.22	0.20	0.18	0.17
XN-80/Skyflex	0.46	0.46	0.46	0.47	0.46	0.40	0.36	0.33	0.30	0.27	0.25	0.23
YSH-70A/Skyflex	0.50	0.50	0.50	0.50	0.50	0.44	0.40	0.36	0.32	0.29	0.27	0.25

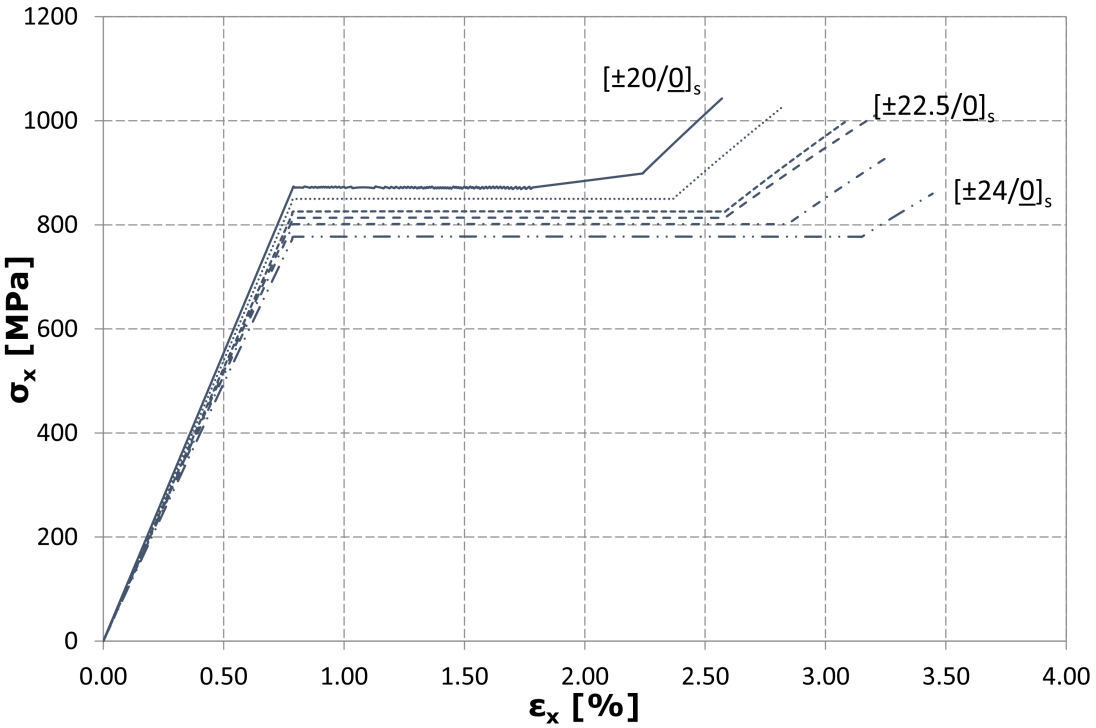

Figure 2: Stress-strain predictions for the M55—Skyflex layups are shown. Over the range of fibre angles, there is considerable increase in ε_d for only a small drop in σ_Y.

Having established the maximum fibre angles for each combination, the model can then be used to predict their stress-strain responses. The model is run for each layup expected to exhibit pseudo-ductility and the results for each material combination are presented alongside each other. Figure 2 shows the behaviour of $[\pm\theta/\underline{0}]_s$ laminates, where θ covers the range 20° – 24°. Table 3 gives the parameters of initial laminate modulus, E_{xi}, strength, σ_x^*, strain to failure, ε_x^*, 'yield' stress, σ_Y and pseudo-ductile strain, ε_d, for each of the fibre angles modelled. The high modulus of the M55J fibres leads to only very slight reductions in E_{xi} as θ is increased. The non-linearity of the $\pm\theta$ plies, observed in [1, 3], is also restricted by these stiff fibres, which is shown by the linear slope up to the point of fragmentation at

$\varepsilon_{frag} = 0.8\%$. Table 3 indicates that the values of σ_Y between $\theta = 20^\circ$ and $\theta = 24^\circ$ are separated by just 93 MPa. Conversely, the ε_x^* increases by 34% from 2.57% for the $[\pm 20/\underline{0}]_s$ to 3.45% for the $[\pm 24/\underline{0}]_s$. This in turn leads to a large increase in ε_d, up to 2.34% for the $[\pm 24/\underline{0}]_s$. The level of pseudo-ductility exhibited by all the layups shown in Figure 2 is extensive, which coupled with strengths in excess of 850 MPa, suggests very promising stress-strain behaviour from this combination.

Covering the same range of fibre angles for the $\pm\theta$ plies, the stress-strain results of layups containing the XN-80 are presented in Figure 3. The values of σ_Y are similar to the M55J layups, the key differences, as shown in Table 4, are the greatly increased E_{xi}. This increase in initial modulus comes at the cost of a lower ε_{frag} of 0.5%, though it is still respectable in terms of aerospace design allowables [20]. Use of the XN-80 fibres also leads to a longer stress plateau whilst fragmentation and dispersed delaminations occur. This has the effect of increasing the amount of pseudo-ductile strain these laminates exhibit compared to those containing the M55J fibres. There is, however, a reduced margin between σ_Y and σ_x^*. This is clear in Figure 3 where, following fragmentation saturation and delamination, there is no further loading before failure of the $[\pm 24/\underline{0}]_s$ layup.

As discussed above, the applicable range of $\pm\theta$ angles for the laminates with YSH-70A fibres is much more extensive than the previous two configurations. The layups between $[\pm 20/\underline{0}]_s$ and $[\pm 25/\underline{0}]_s$ show, in Figure 4, large differences between the σ_Y and σ_{del}. Following fragmentation saturation the stress increases up to σ_{del}, which is the point of gradient increase in the slope up to laminate failure. Mentioned previously, the low value of σ_Y compared to σ_x^* indicates that these layups are not the optimal use of the material. A more efficient response is seen as $\pm\theta$ is increased towards 29° and the relation of σ_Y/σ_x^* moves closer to unity. The compromise between strength and pseudo-ductility is clear — there is a 45% decrease in σ_x^* coupled with a 100% increase in ε_d as $\pm\theta$ increases from 20° to 29°. The use of high modulus fibres means that there is limited reduction in E_{xi} for the same fibre angle increase.

Table 3: Key parameters of initial laminate modulus, E_{xi}, strength, σ_x^*, strain to failure, ε_x^*, 'yield' stress, σ_Y and pseudo-ductile strain, ε_d are presented for each $\pm\theta$ predicted for the M55J—Skyflex.

		20	21	22	22.5	23	24
E_{xi}	[GPa]	110	107	104	103	101	99
σ_x^*	[MPa]	1043	1030	1011	997	931	860
ε_x^*	[%]	2.57	2.83	3.08	3.21	3.26	3.45
σ_Y	[MPa]	874	852	830	818	805	781
ε_d	[%]	1.37	1.62	1.87	1.97	2.10	2.34

Table 4: E_{xi}, σ_x^*, ε_x^*, σ_Y and ε_d are presented for each $\pm\theta$ predicted for the XN-80 — Skyflex.

		20	21	22	22.5	23	24
E_{xi}	[GPa]	156	153	151	150	148	146
σ_x^*	[MPa]	951	934	889	873	804	731
ε_x^*	[%]	2.62	2.84	2.98	3.12	3.12	3.26
σ_Y	[MPa]	791	774	764	758	751	737
ε_d	[%]	1.77	2.00	2.18	2.29	2.37	2.57

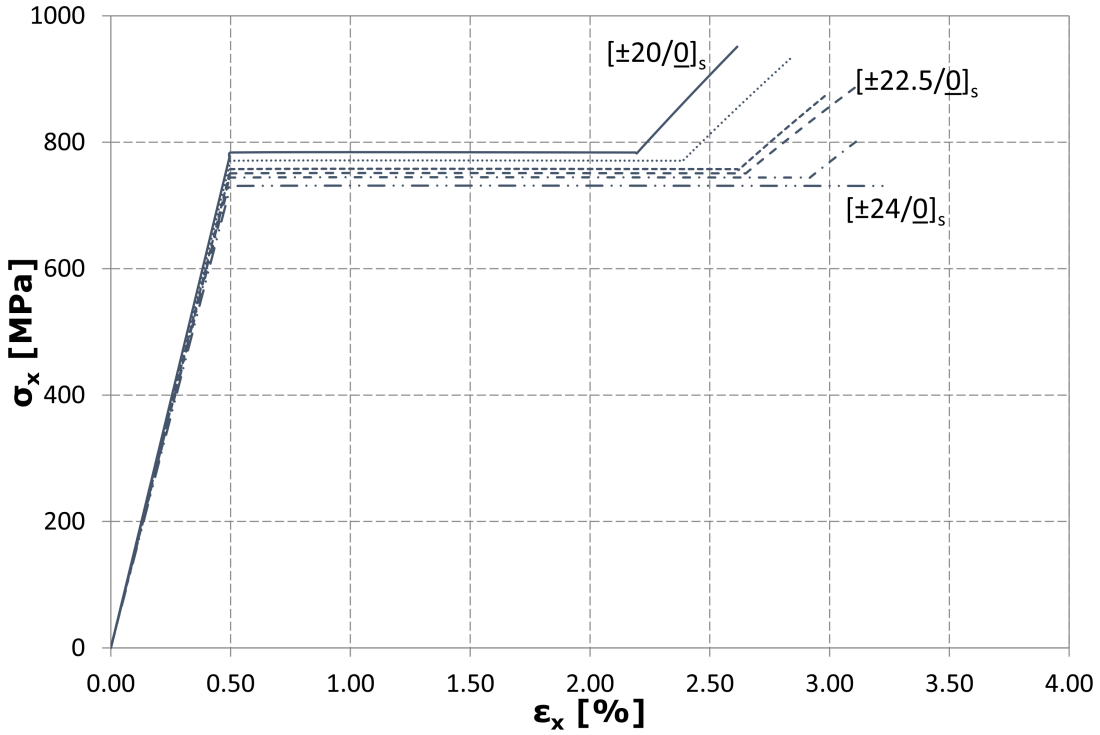

Figure 3: Stress-strain predictions for the XN80—Skyflex layups are shown. The value of σ_Y as a proportion of the laminate strength is high; so much so that the $[\pm 24/\underline{0}]_s$ laminate is predicted to fail without further increase in stress following complete delamination.

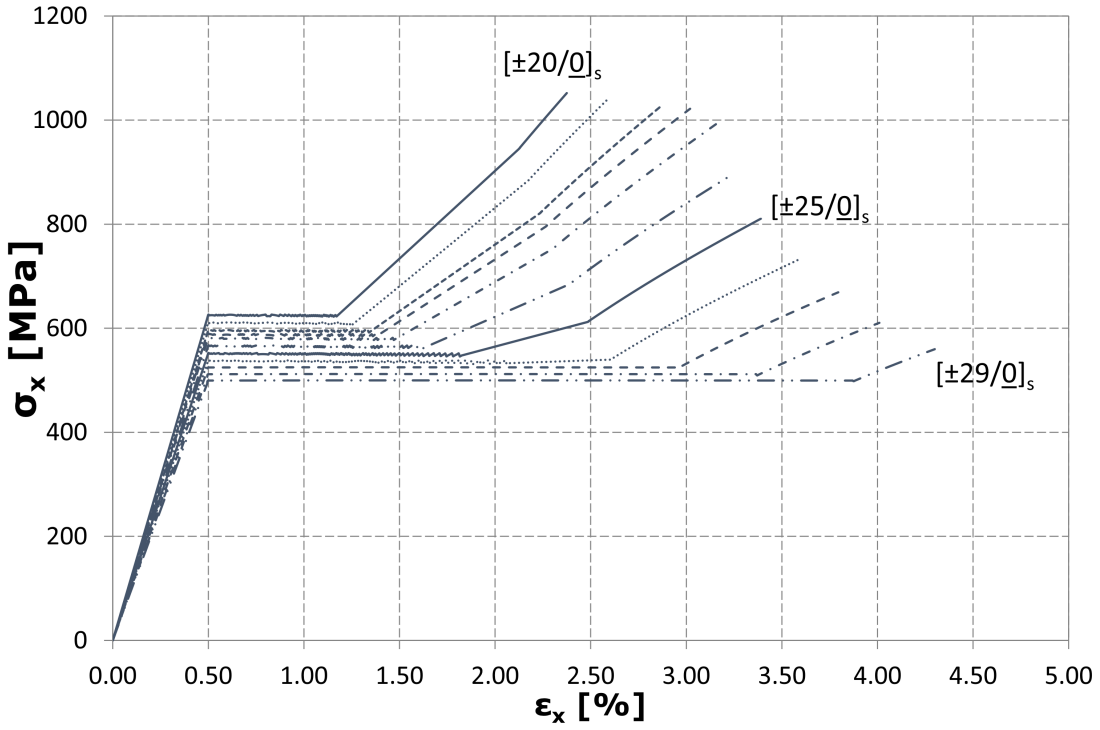

Figure 4: Stress-strain predictions for the YSH-70A—Skyflex layups are shown. The fibre modulus of the YSH70A is lower than that of the XN-80, so for the same fragmentation strain, σ_Y is considerably lower than seen in Figure 3.

Table 5: E_{xi}, σ_x^*, ε_x^*, σ_Y and ε_d are presented for each $\pm\theta$ predicted for the YSH-70A—Skyflex.

		20	21	22	22.5	23	24	25	26	27	28	29
E_{xi}	[GPa]	124	122	119	117	116	113	110	107	105	102	99
σ_x^*	[MPa]	1052	1040	1027	1022	1000	898	811	735	669	610	560
ε_x^*	[%]	2.38	2.59	2.87	3.02	3.19	3.25	3.39	3.61	3.80	4.01	4.30
σ_Y	[MPa]	628	614	599	591	587	569	555	543	529	516	504
ε_d	[%]	1.32	1.52	1.79	1.93	2.10	2.26	2.47	2.75	3.00	3.26	3.60

4 DISCUSSION

The analytical predictions presented above provide, via a straightforward method, some very promising results for exploiting pseudo-ductility. The analysis of $[\pm\theta/\underline{0}]_s$ laminates and the key parameters presented in Tables 3–5 demonstrate the available level of control over the performance. By hybridising the fibre types as discussed, it is possible to define particular characteristics depending on the desired stress-strain behaviour. For example, if a $\sigma_Y > 800$ MPa were required, as Table 3 shows, the M55J fibres would be the selection for the 0° plies, using $\pm\theta$ angles between 20° and 23°. Conversely, if maximisation of ε_d was the requirement, YSH-70A fibres would be selected, as Table 5 shows that pseudo-ductile strains in excess of 3% are achievable with $\pm\theta$ angles of 27°, 28° or 29°. This high strain behaviour leads to a significantly lower σ_Y and σ_x^*, clearly showing that some compromise is inevitable. If the XN-80 fibres are used instead, this trade-off is lessened. Table 4 indicates that σ_Y can be increased whilst achieving a pseudo-ductile strain of over 2% for almost all the $\pm\theta$ angles modelled. These layups have the additional characteristic of an E_{xi} equivalent to the tensile Young's modulus of commercial intermediate modulus CFRP, such as IM7-8552 [21].

The use of different high modulus fibre types each with differing strains to failure allows a range of ε_{frag} to be realised. Failure strains of 0.5% for the XN-80 and YSH-70A and 0.8% for the M55J fibres, give some flexibility when dealing with design requirements for the initial loading of the laminate, before initiation of fragmentation.

The crucial benefit with these configurations, however, is the retention of the initial laminate modulus with increasing pseudo-ductility. There is very little reduction in E_{xi} as $\pm\theta$ is increased, which means that the initial load carrying capability is practical for the laminates displaying even the most pseudo-ductility. In addition to this, the use of thin ply material with thickness between 0.03 mm and 0.046 mm and only five plies per $[\pm\theta/\underline{0}]_s$ layup means that the total laminate thickness (0.150–0.166 mm) is very similar to standard thickness CFRP (0.13 mm). Subsequently, there is considerable potential for these to form pseudo-ductile plies for use in thicker laminates. These plies would also benefit from improved transverse and shear properties compared to standard prepreg tapes, due to the $\pm\theta$ fibre directions.

5 CONCLUSIONS

It has been shown, via a analytical modelling method, that thin ply CFRP $[\pm\theta/\underline{0}]_s$ laminates can exhibit high levels of pseudo-ductility under tensile loading. The metal-like stress-strain curves produced by the modelling, display three main characteristics: initial largely linear response; stress plateau that occurs due to fragmentation and dispersed delamination of the 0° plies, and further loading up to failure. Three different North Thin Ply Technology CFRP materials, each with high modulus carbon fibre types — Toray M55J ($E_f = 540$ GPa), Nippon XN-80 ($E_f = 780$ GPa) and YSH-70A ($E_f = 720$ GPa) — have been used for the 0° plies and hybridised with a Skyflex CFRP containing standard modulus TR30 fibres ($E_f = 235$ GPa). These high modulus fibres have allowed a considerable degree of control over

the stress-strain behaviour of the laminates. Having identified the range of $\pm\theta$ values that will yield pseudo-ductility from each of the fibre combinations, it has been shown that it is possible to effectively 'tune' the stress-strain response. For example, using M55J fibres in a $[\pm 23/\underline{0}]_s$ layup, a σ_Y of 805 MPa, ε_d of 2.1% and σ_x^* of 931 MPa can be achieved. If the same angle-ply layup is used, but combined with YSH-70A fibre 0° plies, the same ε_d is given but the 'yield' and strength values change markedly to 587 MPa and 1000 MPa respectively. Thus it is possible to select the parameter for maximisation, ε_d, σ_Y or σ_X^* and pick a fibre type and $\pm\theta$ layup that will be optimal for each.

This concept offers particular promise in producing pseudo-ductile stress-strain behaviour using thin ply CFRP laminates. Experimental testing of a selection of these laminates is ongoing, in order to establish both the accuracy of the modelling and potential for further investigations into this concept.

ACKNOWLEDGEMENTS

This work was funded under the UK Engineering and Physical Sciences Research Council (EPSRC) Programme Grant EP/I02946X/1 on High Performance Ductile Composite Technology in collaboration with Imperial College, London.

References

[1] J. D. Fuller, M. R. Wisnom, Pseudo-ductility and damage suppression in thin ply CFRP angle-ply laminates, Composites Part A: Applied Science and Manufacturing 69 (2014) 64–71. doi:10.1016/j.compositesa.2014.11.004.

[2] G. Czél, M. R. Wisnom, Demonstration of pseudo-ductility in high performance glass/epoxy composites by hybridisation with thin-ply carbon prepreg, Composites Part A: Applied Science and Manufacturing 52 (2013) 23–30. doi:10.1016/j.compositesa.2013.04.006.

[3] J. D. Fuller, M. Jalalvand, M. R. Wisnom, Pseudo-Ductility by Fragmentation of Central Unidirectional Plies in Thin CFRP Angle-Ply Laminates, in: 16th European Conference on Composite Materials, Seville, 2014.

[4] J. D. Fuller, M. R. Wisnom, Exploration of the potential for pseudo-ductility in thin ply CFRP angle-ply laminates via an analytical method, Composites Science and Technology 112 (2015) 8–15. doi:10.1016/j.compscitech.2015.02.019.

[5] M. Jalalvand, G. Czél, M. R. Wisnom, Damage analysis of pseudo-ductile thin-ply UD hybrid composites – A new analytical method, Composites Part A: Applied Science and Manufacturing 69 (2015) 83–93. doi:10.1016/j.compositesa.2014.11.006.

[6] T. O'Brien, Characterisation of delamination onset and growth in a composite laminate, Tech. rep., NASA, Langley (1981).

[7] A. Wang, F. Crossman, Initiation and Growth of Transverse Cracks and Edge Delamination in Composite Laminates Part 1. An Energy Method, Journal of Composite Materials 14 (1) (1980) 71–87.

[8] D. Leguillon, G. Marion, R. Harry, F. Lecuyer, The onset of delamination at stress-free edges in angle-ply laminates—analysis of two criteria, Composites Science and Technology 61 (2001) 0–5.

[9] C. T. Herakovich, Influence of Layer Thickness on the Strength of Angle-Ply Laminates, Journal of Composite Materials 16 (3) (1982) 216–227.

[10] G. Czél, M. Jalalvand, M. R. Wisnom, Demonstration of pseudo-ductility in unidirectional hybrid composites made of discontinuous carbon/epoxy and continuous glass/epoxy plies, Composites Part A: Applied Science and Manufacturing 72 (2015) 75–84. doi:10.1016/j.compositesa.2015.01.019.

[11] J. Aveston, G. A. Cooper, A. Kelly, Single and multiple fracture, in: The Properties of Fibre Composites, National Physics Laboratory, National Physical Laboratory, Guildford, 1971, pp. 15—-25.

[12] A. R. Bunsell, B. Harris, Hybrid carbon and glass fibre composites, Composites 5 (4) (1974) 157–164. doi:10.1016/0010-4361(74)90107-4.

[13] Y. Swolfs, L. Gorbatikh, I. Verpoest, Fibre hybridisation in polymer composites: A review, Composites Part A: Applied Science and Manufacturing 67 (2014) 181–200. doi:10.1016/j.compositesa.2014.08.027.

[14] TorayCA, TORAY M55J DATA SHEET.

[15] Nippon Graphite Fiber Corporation, Nippon Granoc Yarn XN Series (2010).

[16] Nippon Graphite Fiber Corporation, Nippon Granoc Yarn YSH-A Series (2010).

[17] J. D. Fuller, M. Jalalvand, M. R. Wisnom, Damage mechanisms of pseudo-ductile thin ply angle-ply laminates containing central 0° plies, Submitted to Composite Structures.

[18] W. Cui, M. Wisnom, M. Jones, An experimental and analytical study of delamination of unidirectional specimens with cut central plies, Journal of Reinforced Plastics and . . . 13.

[19] R. Amacher, J. Cugnoni, J. Botsis, L. Sorensen, W. Smith, C. Dransfeld, Thin ply composites: Experimental characterization and modeling of size-effects, Composites Science and Technology 101 (2014) 121–132. doi:10.1016/j.compscitech.2014.06.027.

[20] M. Price, A. Murphy, J. Butterfield, B. . Falzon, D. Quinn, Integrating allowable design strains in composites with whole life value, Procedia CIRP 11 (2013) 278—-283.

[21] S. Hallett, B. Green, W. Jiang, M. Wisnom, An experimental and numerical investigation into the damage mechanisms in notched composites, Composites Part A: Applied Science and Manufacturing 40 (5) (2009) 613–624. doi:10.1016/j.compositesa.2009.02.021.